The z-GAL survey

S. Berta[1,*], P. Cox[2], D. Ismail[3], and the z-GAL collaboration

[1]Institut de Radioastronomie Millimétrique (IRAM), 300 rue de la Piscine, 38400 Saint-Martin-d'Hères, France
[2]Sorbonne Université, UPMC Université Paris 6 and CNRS, UMR 7095, Institut d'Astrophysique de Paris, 98b boulevard Arago, 75014 Paris, France
[3]Aix-Marseille Université, CNRS and CNES, Laboratoire d'Astrophysique de Marseille, 38 rue Frédéric Joliot-Curie, 13388 Marseille, France

Abstract.
The z-GAL survey observed 137 bright *Herschel*-selected galaxies with the IRAM Northern Extended Millimeter Array (NOEMA) to measure their spectroscopic redshift. It detected several multiple sources and secured the spectroscopic redshift of a total of 165 individual galaxies over the range $0.8 < z < 6.5$. The wealth of information provided by the NOEMA spectra allowed us to study the physical properties of these galaxies. By modelling their spectral energy distributions, we determined their dust mass, $M_{\rm dust}$, temperature, $T_{\rm dust}$, and emissivity index, $\beta_{\rm dust}$ and found a significant anti-correlation between $T_{\rm dust}$ and $\beta_{\rm dust}$. Using the detected ^{12}CO lines, we derived the molecular gas mass of the z-GAL sources. Combining the molecular lines and the dust continuum emission, we computed their gas depletion timescales, $\tau_{\rm dep}$: the z-GAL sample consists mainly of powerful starbursts with $\tau_{\rm dep}$ in the range between 0.1 and 1.0 Gyr, while only $\sim 25\%$ belongs to the 'main sequence' of star forming galaxies.

1 Introduction: The path to z-GAL

In the early Universe, the bulk of star formation occured in dusty star-forming galaxies (DSFGs) [1–3]. Galaxy growth, traced by the cosmic star formation density (SFRD), peaked at redshifts $1 < z < 3$ [see the review by 4]. *Spitzer* and *Herschel* extragalactic surveys showed that galaxies with IR luminosity $L_{\rm IR} < 10^{11}\,L_{\odot}$ dominate the cosmic SFRD in the local Universe, luminous infrared galaxies (LIRGs, $L_{\rm IR} > 10^{11}\,L_{\odot}$) dominate at redshift $z > 1$, and ultra-luminous infrared galaxies (ULIRGs, $L_{\rm IR} > 10^{12}\,L_{\odot}$) at $z > 2$ [5, 6].

In the stellar mass versus star formation rate (SFR) space, star-forming galaxies are preferentially found on the so-called 'main sequence' (MS)[e.g. 7–10]. For a given stellar mass, the SFR of the MS increases at earlier cosmic times [9]. Galaxies lying above the MS are starbursts, possibly triggered by interactions and mergers with other galaxies. MS galaxies evolve secularly, with a regular star formation activity [11, 12]. Because of the evolution of the MS, a SFR $\sim 100\,M_{\odot}$/yr galaxy is a powerful starburst in the local Universe, but is a MS galaxy at $z > 2$ [13, 14]. The cosmic SFRD is thus dominated by MS galaxies from $z = 0$ at least up to $z \sim 3$. The contribution of starbursts is instead only ~5-10% of the SFRD [15, 16].

*e-mail: berta@iram.fr

Combining *Herschel* [17, 18], *Planck* [19] and South Pole Telescope (SPT) [20] surveys, large samples of luminous DFSGs have been built, with IR luminosities reaching $10^{13}\,L_{\odot}$, corresponding to SFR $\sim 1000\,M_{\odot}$ yr^{-1}, including strongly lensed systems and rare cases of hyper-luminous infrared galaxies (HyLIRGs) [21–26].

A detailed study of the physical nature of these sources requires an accurate measurement of their distance. Because of their intrinsic heavy dust absorption, optical and near-infrared spectroscopy is not successful for most of these objects, even with the largest ground-based facilities. Photometric redshifts based on far-infrared and sub-millimetre continuum data are also very uncertain. Therefore sub-millimetre and millimetre spectroscopy is the most reliable method to secure redshifts for these high-z dust-obscured objects.

The IRAM Northern Extended Millimetre Array (NOEMA) and the Atacama Large Millimetre/submillimetre Array (ALMA) play a central role in studying high-z DSFGs selected from wide field surveys at shorter wavelengths. To date, spectroscopic campaigns carried out with ALMA, NOEMA and with single-dish telescopes (e.g. IRAM 30m, GBT, APEX, and LMT) measured precise redshifts for a total of ~150 such sources [e.g. 27–32].

The NOEMA PolyFiX correlator, with a total bandwidth of 31 GHz, is the optimal instrument for sub-mm spectral scans aimed at determining the redshift of distant galaxies. A Pilot Programme successfully demonstrated this by measuring the redshift of 11 bright *Herschel* galaxies in the North Galactic Pole (NGP) H-ATLAS field [33].

Building upon the success of the Pilot Programme, the z-GAL project observed 126 *Herschel*-selected bright DSFGs (with $S_{500\mu\mathrm{m}} \geq 80$ mJy) in the NGP H-ATLAS and equatorial HeLMS and HerS fields. The first results of the z-GAL survey are presented in three papers: [34] describes the survey and reports on the measurement of the spectroscopic redshifts; [35] discusses the dust continuum properties of the sources; [36] reports on the physical properties of the sources, as inferred from the molecular and atomic gas lines (^{12}CO, [CI], and H_2O) and dust, and discusses molecular gas masses and depletion timescales. Finally [37] will report on the nature of the sources and will compare the NOEMA data to the available ancillary information.

2 Spectroscopic redshift and line properties

The main goal of z-GAL is to measure the spectroscopic redshift of the targets. Based on the detection of at least two emission lines, robust spectroscopic redshifts have been determined for 135 out of the 137 observed sources (including the Pilot Programme). The main detected spectral lines are ^{12}CO transitions from $(2-1)$ to $(8-7)$ and occasionally those of H_2O, [CI], and HCN/HCO$^+$. For several targets, NOEMA detected multiple sources, for a total of 165 individual galaxies with spectroscopic confirmation, thus more than doubling the total number of high-z galaxies with available sub-millimetre and millimetre spectroscopic redshift. The z-GAL galaxies lie in the redshift range $0.8 < z < 6.5$, with a median of $z = 2.56 \pm 0.10$. The left-hand panel of Fig. 1 presents the redshift distribution of the z-GAL galaxies.

The line widths of the z-GAL are very broad, with ~ 35% of them having a full width at half maximum (FWHM) of $\Delta V \geq 700$ km s^{-1}, extending up to 1800 km s^{-1}. The right-hand panel of Fig. 1 shows their FWHM distribution. Many of the broad lines show profiles that are asymmetrical or double-peaked, with separation between the peaks of up to a few 100 km s^{-1}, indicative of merger systems and/or rotating disks [34]. The reason of these very broad lines will be further discussed in [37].

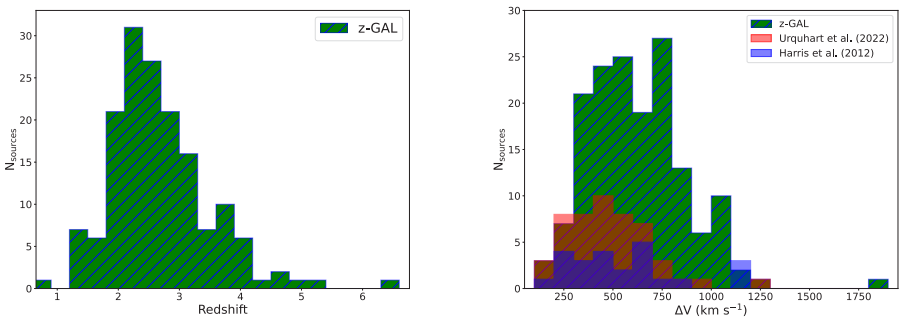

Figure 1. Spectral lines properties of all 165 z-GAL individual galaxies (courtesy of [34]). *Left*: distribution of spectroscopic redshift. *Right*: distribution of the lines FWHM. For comparison, the FWHM distribution of other *Herschel*-selected sources reported by [32, 38] are shown as blue and red histograms, respectively.

3 Dust continuum and SED properties

The continuum flux densities of the z-GAL sources were extracted from up to ten sidebands over the frequency range from 76.3 to 206.5 GHz. All sources were detected in at least four continuum sidebands, finely sampling the Rayleigh-Jeans tail of their dust spectral energy distributions (SEDs). [35] presents the continuum SEDs of the z-GAL survey, including *Herschel*, SCUBA2 and NOEMA data, and reproduce them with a modified black body (MBB) in its general form and in the optically thin approximation. The main products of the SED fitting are the dust mass $M_{\rm dust}$, temperature $T_{\rm dust}$ and emissivity index $\beta_{\rm dust}$ of the sources. With the aim of tracing how the results are affected by possible missing data and model-dependent effects, [35] produced a mock catalog and fitted it with the same MBB models.

In order to ease the comparison between z-GAL results and the literature, the optically thin results were chosen as reference. Figure 2 presents examples of SED fitting for the z-GAL pilot sources. The effects of assuming a MBB in its general form are discussed by [35]: dust temperature increases by $\sim$ 20% with respect to the optically-thin approximation. The mock analysis shows that accurate $T_{\rm dust}$ values can be estimated using the general MBB only if the source size is known. On the other hand, basing the fit on the use of the wavelength at which dust becomes optically thick ($\lambda_{\rm thick}$), the results still suffer from strong degeneracies and can overestimate $T_{\rm dust}$ by up to $\sim$ 20%, thus underestimating $M_{\rm dust}$ by up to 40%.

A significant anti-correlation between β and $T_{\rm dust}$ was found (Fig. 3). It can be reproduced by a function of the form $\beta \propto T_{\rm dust}^{-\alpha}$, with $\alpha = 0.69 \pm 0.04$. The mock analysis indicates that such anti-correlation is not induced by either the sample selection or the fitting method. Further investigations are needed to study in detail its implications and its cause.

4 Molecular gas mass and depletion time scales

A total of 358 emission lines were detected in the whole z-GAL sample (including the Pilot Programme) probing the molecular gas (^{12}CO and H_2O), as well as – for a few sources – the atomic gas ([CI]) [36]. Using the detected ^{12}CO lines and typical typical line luminosity ratios of sub-millimetre galaxies (SMGs) [40], [36] computed the ^{12}CO(1 – 0) luminosities of the z-GAL sources and converted them into molecular gas masses, $M_{\rm mol}$, adopting a conversion factor $\alpha_{\rm CO} = 4.0\ {\rm M}_\odot\ ({\rm K\ km\ s^{-1}\ pc^2})^{-1}$ [41].

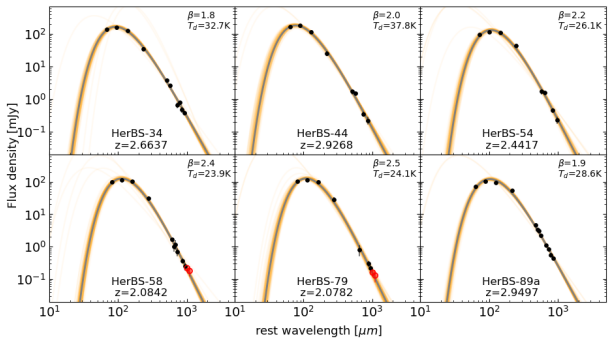

Figure 2. SED fitting of z-GAL pilot sources (adapted from [35]). Black dots represent the data effectively fitted by the model; data points at $\lambda > 1000\,\mu$m (restframe) are represented with open, red symbols. The best fit optically-thin MBB model is the solid grey line. The orange lines are the output sampling of 100 random walks extracted from the Monte Carlo results, showing the robustness of the fit.

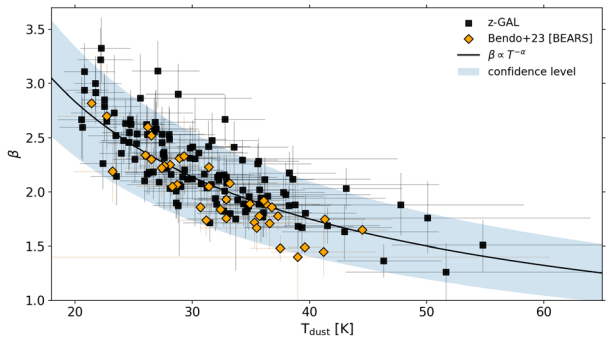

Figure 3. $\beta - T_{\rm dust}$ anti-correlation for the z-GAL sources (black squares) compared to the BEARS sources (orange diamonds, [39]). The solid black line is the fitted relation we find for the z-GAL sources with $\alpha = 0.69 \pm 0.04$ and the shaded region is the corresponding confidence level. Adapted from [35].

For comparison, $M_{\rm mol}$ was also derived from the available [CI] transitions and from the 850 μm rest-frame dust continuum. The former produced an estimate of $M_{\rm mol}$ consistent with ^{12}CO within a factor $\sim$ 1.5. The latter gave results consistent with ^{12}CO within ±50% for only half of the z-GAL sample.

Combining the information derived from the ^{12}CO lines [36] and from SED fitting [35], we obtained a median gas-to-dust mass ratio, $\delta_{\rm GDR}$, of 107 ± 50 for the z-GAL sample, consistent with the values of star-forming galaxies of nearly solar metallicity.

Moreover we built the integrated Kennicutt-Schmidt relation (KS) [42, 43], linking the ongoing SFR of the z-GAL galaxies to their molecular gas reservoir (Fig. 4, left panel). The z-GAL sources sample well the brightest luminosity ($\mu L_{\rm IR} > 10^{13}$ L$_\odot$) and most massive ($M_{\rm mol} > 10^{11}$ M$_\odot$) end of the KS plane, bridging the loci of high-z lensed galaxies and unlensed ULIRGs.

The depletion timescale, $\tau_{\rm dep} = \mu M_{\rm mol}/\mu$SFR is independent of possible lensing magnification (assuming no differential effects). The right-hand panel of Fig. 4 compares the $\tau_{\rm dep}$ distribution of the z-GAL galaxies to that of other samples. The z-GAL sources have $\tau_{\rm dep}$ in the range between 0.1 and 1.0 Gyr and are located between the star forming MS and the locus of starbursts.

5 Conclusion

Thanks to the very broad bandwidth of NOEMA, the z-GAL survey measured the spectroscopic redshift of 165 high-z galaxies in the range $0.8 < z < 6.5$, in the fields of 135 bright distant *Herschel*-selected sources, thus more than doubling the number of distant SMGs with available precise redshift. The sample includes gravitationally-lensed galaxies, and non-

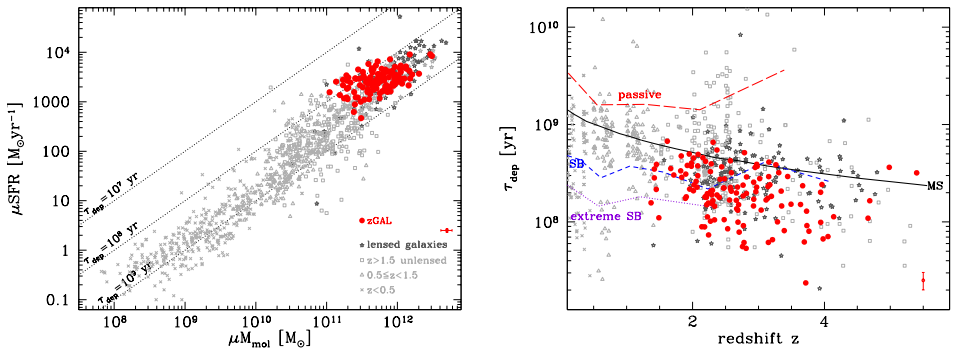

Figure 4. Physical nature of the *z*-GAL sources (adapted from [36]). *Left*: integrated Kennicutt-Schmidt relation. Red symbols represent the *z*-GAL sources, including the Pilot Programme. The typical error bar is shown at the bottom-right. The loci of constant $\tau_{\rm dep}$ are traced as dotted lines. Literature data include the collection by [44] and data by [45–47]; a full list is in [36]. *Right*: depletion timescale as a function of redshift. The different lines represent the trends of different classes of galaxies [44].

lensed sources, possible proto-cluster members, confirmed AGNs, multiple systems, interacting pairs, and rare isolated HyLIRGs [34–37].

Despite this heterogeneity, the majority of the *z*-GAL galaxies are powerful starbursts, destined to exhaust their molecular gas reservoir over timescales of few 10^8 years. The most powerful of these sources host among the most intense bursts of star formation recorded ($\tau_{\rm dep} < 10^8$ yr). Interestingly, $\sim 25\%$ of the *z*-GAL galaxies belong to the main sequence of star formation, where galaxies undergo a secular evolution.

More data spanning over the whole electromagnetic spectrum from the x-rays to the radio frequencies, including high resolution optical and mid-IR imaging and spectroscopy, are required to ultimately characterise the intriguing *z*-GAL galaxies.

Acknowledgements

The success of the *z*-GAL survey would have not been possible without the invaluable work of the *z*-GAL Cat Team and Tiger Team, who performed the calibration, reduction and delivery of the *z*-GAL data. This work is based on observations carried out under project numbers M18AB and D20AB with the IRAM NOEMA Interferometer. IRAM is supported by INSU/CNRS (France), MPG (Germany) and IGN (Spain). The authors are grateful to IRAM for making this work possible and for the continuous support that they received over the past four years to make this large programme a success. The authors are also grateful to the IRAM director for approving the DDT proposal that enabled to complete the survey.

References

[1] R.J. Bouwens, M. Aravena, R. Decarli et al., ApJ **833**, 72 (2016)
[2] J.S. Dunlop, R.J. McLure, A.D. Biggs et al., MNRAS **466**, 861 (2017)
[3] J.A. Zavala, C.M. Casey, S.M. Manning et al., ApJ **909**, 165 (2021)
[4] P. Madau, M. Dickinson, ARA&A **52**, 415 (2014)
[5] B. Magnelli, D. Elbaz, R.R. Chary et al., A&A **528**, A35 (2011)
[6] B. Magnelli, P. Popesso, S. Berta et al., A&A **553**, A132 (2013)

[7] R. Guzmán, J. Gallego, D.C. Koo et al., ApJ **489**, 559 (1997)
[8] J. Brinchmann, R.S. Ellis, ApJ **536**, L77 (2000)
[9] D. Elbaz, E. Daddi, D. Le Borgne et al., A&A **468**, 33 (2007)
[10] E. Daddi, M. Dickinson, G. Morrison et al., ApJ **670**, 156 (2007)
[11] A. Saintonge, D. Lutz, R. Genzel et al., ApJ **778**, 2 (2013)
[12] L.J. Tacconi, R. Genzel, A. Saintonge et al., ApJ **853**, 179 (2018)
[13] D. Elbaz, H.S. Hwang, B. Magnelli et al., A&A **518**, L29 (2010)
[14] R. Nordon, D. Lutz, L. Shao et al., A&A **518**, L24 (2010)
[15] G. Rodighiero, E. Daddi, I. Baronchelli et al., ApJ **739**, L40 (2011)
[16] C. Schreiber, M. Pannella, D. Elbaz et al., A&A **575**, A74 (2015)
[17] S. Eales, L. Dunne, D. Clements et al., PASP **122**, 499 (2010)
[18] S.J. Oliver, J. Bock, B. Altieri et al., MNRAS **424**, 1614 (2012)
[19] Planck Collaboration, P.A.R. Ade, N. Aghanim et al., A&A **582**, A29 (2015)
[20] J.D. Vieira, T.M. Crawford, E.R. Switzer et al., ApJ **719**, 763 (2010)
[21] M. Negrello, R. Hopwood, G. De Zotti et al., Science **330**, 800 (2010)
[22] H. Nayyeri, M. Keele, A. Cooray et al., ApJ **823**, 17 (2016)
[23] T.J.L.C. Bakx, S.A. Eales, M. Negrello et al., MNRAS **473**, 1751 (2018)
[24] R.J. Ivison, A.M. Swinbank, I. Smail et al., ApJ **772**, 137 (2013)
[25] D.A. Riechers, C.M. Bradford, D.L. Clements et al., Nature **496**, 329 (2013)
[26] L. Wang, F. Gao, P.N. Best et al., A&A **648**, A8 (2021)
[27] A. Weiß, C. De Breuck, D.P. Marrone et al., ApJ **767**, 88 (2013)
[28] R. Cañameras, N.P.H. Nesvadba, D. Guery et al., A&A **581**, A105 (2015)
[29] C. Reuter, J.D. Vieira, J.S. Spilker et al., ApJ **902**, 78 (2020)
[30] J.E. Birkin, A. Weiss, J.L. Wardlow et al., MNRAS **501**, 3926 (2021)
[31] K.C. Harrington, A. Weiss, M.S. Yun et al., ApJ **908**, 95 (2021)
[32] S.A. Urquhart, G.J. Bendo, S. Serjeant et al., MNRAS **511**, 3017 (2022)
[33] R. Neri, P. Cox, A. Omont et al., A&A **635**, A7 (2020)
[34] P. Cox, R. Neri, S. Berta et al., A&A in press, arXiv:2307.15732 (2023)
[35] D. Ismail, A. Beelen, V. Buat et al., A&A in press, arXiv:2307.15747 (2023)
[36] S. Berta, F. Stanley, D. Ismail et al., A&A in press, arXiv:2307.15748 (2023)
[37] T. Bakx, A. Baker, P. Cox et al., A&A (in preparation)
[38] A.I. Harris, A.J. Baker, D.T. Frayer et al., ApJ **752**, 152 (2012)
[39] G.J. Bendo, S.A. Urquhart, S. Serjeant et al., MNRAS **522**, 2995 (2023)
[40] C.L. Carilli, F. Walter, ARA&A **51**, 105 (2013)
[41] L. Dunne, S.J. Maddox, P.P. Papadopoulos et al., MNRAS **517**, 962 (2022)
[42] M. Schmidt, ApJ **129**, 243 (1959)
[43] J. Kennicutt, Robert C., ApJ **498**, 541 (1998)
[44] L.J. Tacconi, R. Genzel, A. Sternberg, ARA&A **58**, 157 (2020)
[45] C. Yang, A. Omont, A. Beelen et al., A&A **608**, A144 (2017)
[46] T.J.L.C. Bakx, H. Dannerbauer, D. Frayer et al., MNRAS **496**, 2372 (2020)
[47] M. Hagimoto, T.J.L.C. Bakx, S. Serjeant et al., MNRAS **521**, 5508 (2023)